JOURNAL OF SOLID STATE CHEMISTRY 16, 413–422 (1976)

Electrical Properties of Undoped and Doped Potassium Tetrafluoaluminate: $KAlF_4$

J. SCHOONMAN* AND R. A. HUGGINS

Center for Materials Research, Stanford University, Stanford, California

Received January 13, 1975; in revised form July 7, 1975

The electrical conductivity of nominally pure $KAlF_4$ crystals and of nominally pure and doped polycrystalline $KAlF_4$ samples has been studied. The electrical conductivity is highly anisotropic. Intrinsic defects are generated according to a Frenkel mechanism in the potassium ion sublattice. Although BaF_2 and ZrF_4 increase the conductivity due to an increase in potassium ion vacancy concentration, deviations from stoichiometry may lead to fluoride conduction in the extrinsic conductivity region.

1. Introduction

Several ternary alkali fluoaluminates have interesting crystal structures, i.e., layer, channel, and framework structures. The tetrafluoaluminates adopt later structures, whereas the pentafluoaluminates crystallize in channel structures. Some of the alkali fluoaluminates with general composition M_3AlF_6 exhibit structural transformations. For Na_3AlF_6 the transformation is known to be accompanied by an increase in the ionic conductivity (*1*). Upon doping with CaF_2 the conductivity of Na_3AlF_6 increases (*2*). In order to enhance the solubility of CaF_2 in Na_3AlF_6 an excess of AlF_3 has to be added as well (*2*). However, the influence of the composition upon the measured conductivity does not clarify the identity of the conducting species (*3*).

Alkali fluoaluminates do not contain easily reducible species, and therefore, it is expected that electronic conduction in these materials is very low. The present paper deals with the electrical properties of nominally pure and deliberately doped potassium tetrafluoaluminate, $KAlF_4$, which crystallizes in a tetragonal layered structure (*4*). In this material the AlF_4^- layers consist of aluminum ions octahedrally surrounded by fluoride ions, the octahedra being corner-shared. The AlF_4^- layers sandwich layers of potassium ions in a square-planar arrangement with each potassium ion surrounded by eight fluoride ions. This crystal structure suggests an anisotropic electrical conductivity.

The unit cell is illustrated in Fig. 1 (*5*). The unit cell dimensions of the tetragonal structure are $a_0 = 3.550$ Å, $c_0 = 6.138$ Å, and the ions are in the following positions of $D'_{4h}(P4/mmm)$: K, (000); Al, $(\frac{1}{2}\ \frac{1}{2}\ \frac{1}{2})$; F_1, $(0\ \frac{1}{2}\ \frac{1}{2})$ $(\frac{1}{2}\ 0\ \frac{1}{2})$; and F_2, $(\frac{1}{2}\ \frac{1}{2}\ u)$ $(\frac{1}{2}\ \frac{1}{2}\ \bar{u})$, with $u = 0.21$. In order to help elucidate the transport mechanisms in this structure, samples were prepared that were doped with either BaF_2 (and AlF_3) or ZrF_4.

It was expected that the barium ions would reside in the potassium ion sites and that zirconium ions would replace aluminum ions in the octahedral sites, thus increasing the potassium vacancy concentration.

2. Experimental Aspects

A. Sample Preparation

Following the method of Brosset (*4*), $KAlF_4$ was prepared by adding stoichiometric amounts of KHF_2 solution (obtained

* Present address: Solid State Department, State University of Utrecht, Sorbonnelaan 4, Utrecht-De Uithof, The Netherlands.

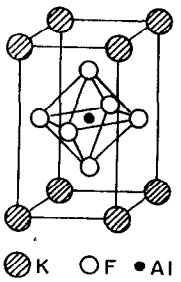

FIG. 1. The unit cell of $KAlF_4$.

by dissolving KF in concentrated HF) to a solution of AlF_3 in aqueous HF (obtained by dissolving $Al(OH)_3$ in concentrated HF). According to the literature (*4*), evaporating the resultant suspension to dryness at about 100°C gives an intermediate precipitate, which consists mainly of $K_2AlF_5 \cdot H_2O$. $KAlF_4$ was obtained upon melting this precipitate at about 625°C for about 15 min, the melting temperature of $KAlF_4$ being 574 ± 1°C. Fusions were carried out in platinum beakers in air. Small optically clear single crystals of undoped $KAlF_4$ were obtained on cooling such a melt at a rate of 0.7°C/min.

Samples have also been prepared of $KAlF_4$ doped with zirconium fluoride and with barium fluoride–aluminum fluoride mixtures. It is expected that the solubility of BaF_2 increases in the presence of a proper proportion of AlF_3. Both $KAlF_4$–ZrF_4 and $KAlF_4$–BaF_2 were prepared by mixing the dopants with the intermediate precipitate, and a subsequent fusion of the mixture in air ($T \cong 750$°C for $\frac{1}{2}$–1 hr). In one preparation, ZrF_4 was added to the AlF_3–HF solution, which should lead to the doped intermediate precipitate. A part of this material was melted under HF for 2 hr at about 800°C. The $KAlF_4$ samples were finely ground in a mortar and pellets were pressed at a pressure of 5.1×10^4 psi. No binder was found to be necessary. After pressing, the pellets were heated for 16 hr in a dry oxygen-free argon stream at 450°C.

X-ray diffraction and ir absorption studies were performed in order to characterize the resulting materials.

The barium content of the samples was determined by atomic absorption spectroscopy, whereas X-ray fluorescence analysis was used to obtain the zirconium content. A series of $KAlF_4$–ZrF_4 mixtures close to the composition of the samples was prepared for use as standards in this analysis.

B. Electrical Conductivity Measurements

Pressed pellets with sputtered platinum electrodes (thickness, 1000 Å) were spring-loaded between two platinum sheets in an evacuable stainless steel conductivity cell.

The a-c electrical conductivity was studied as a function of temperature, frequency, and a-c amplitude, using an a-c impedance bridge (GR 1608 A and GR 1603 A) over the range 0.2–20 kHz. The d-c conductivity values were measured with a Keithley electrometer using a dry cell as a constant voltage source. All measurements were made with the sample under vacuum.

The conductivity was found to behave reproducibly on both heating and cooling in the range 25–430°C. However, small hysteresis effects in the temperature dependence were observed with samples which were heated to about 510°C. A slight increase in conductivity on cooling was accompanied by small weight losses of the samples. The electrical conductivity also behaved reproducibly in the temperature region 25–430°C when the pellets were preheated in an argon flow at temperatures of 250 to 400°C, indicating that the hysteresis effects can be ascribed to evaporation losses which occur at temperatures greater than 430°C. Weight losses were significantly smaller when a pellet was heated to about 500°C in the presence of KF. Above 430°C, a thermodynamically well-defined ambient is evidently required. Both P_{F_2} and the activity of KF, for instance, should be fixed. However, our conductivity cell was not suitable for this type of experiment.

Transference numbers for potassium ions were determined using pellets of KCl doped with $BaCl_2$ as a protective electrolyte. A schematic diagram of the pellet arrangement is shown in Fig. 2. Should t_{K^+} be smaller than 1, then the decrease in weights of pellets 3 and 4 must equal the increase in weight of pellets

$$-Pt|AgI|Ag|X|X|X|Y|Y|Y|X|X|X|Pt+$$
$$1\ 2\ 3\ 4\ 5\ 6\ 7\ 8\ 9$$
$$X = KCl\text{–}BaCl_2, \qquad Y = KAlF_4\text{–}ZrF_4 \quad (2)$$

FIG. 2. Pellet arrangement for transference number measurements.

6 and 7. Under the assumption that $t_{K^+} + t_{F^-} = 1$, the weight changes are given by

$$\Delta W(6,7) = |\Delta W(3,4)| = t_{F^-}(A_K + A_F)\, q/96500, \quad (1)$$

where A_i denotes the atomic weight of species i, q can be calculated from the decrease in weight of the silver electrode.

3. Experimental Results

A. Materials Characterization

The X-ray diffraction pattern of the dried intermediate precipitate revealed the presence of $K_2AlF_5 \cdot H_2O$, AlF_3, $KAlF_4$, and KHF_2, which indicates the following reaction scheme in aqueous solution,

$$2KHF_2 + 2Al(OH)_3 + 4HF = K_2AlF_5 \cdot H_2O + AlF_3 + 5H_2O, \quad (2)$$

whereas to some extent the reaction

$$KHF_2 + Al(OH)_3 + 2\ HF = KAlF_4 + 3H_2O \quad (3)$$

has also occurred. Upon subsequent melting $KAlF_4$ results, according to (*4*).

$$K_2AlF_5 \cdot H_2O + AlF_3 \xrightarrow{270°C} K_2AlF_5 + AlF_3 + H_2O\uparrow = 2KAlF_4. \quad (4)$$

The X-ray diffraction results are gathered in Table I.

Since the potassium fluoaluminates were prepared from aqueous solutions, contamination by OH^- ions cannot be ruled out. The optical absorption of both undoped and doped samples was investigated in the region 600–4000 cm^{-1}. The sample materials were mixed with dried KBr and pellets were pressed in an evacuable die. The results are presented in Table II.

According to Lecompte et al. (*6*), band C can be assigned to ν_3 of the octahedra in the AlF_4^-layers. These authors, using Brosset's method of preparation, investigated the spectral region 300–1500 cm^{-1}. The OH^- bands appear at larger wavenumbers.

Fusion under HF evidently did not completely prevent the incorporation of OH^- ions. In the spectral region investigated, ZrF_4 shows a band at 668 cm^{-1}, AlF_6^{3-}, if present in $KAlF_4$, would show a band at 646 cm^{-1} (*7*), whereas BaF_2 would show bands at 720 and 1340 cm^{-1}. None of these bands were present in the recorded spectra.

The atomic absorption spectroscopy analyses revealed the presence of 0.016 mole

TABLE I

COMPOSITION OF THE POTASSIUM FLUOALUMINATES[a]

Material	$K_2AlF_5 \cdot H_2O$	KHF_2	AlF_3	$KAlF_4$	K_3AlF_6	ZrF_4	BaF_2
I	X	X	X	X			
$KAlF_4$				X			
$KAlF_4$–ZrF_4(1)				X		n.d.	
$KAlF_4$–BaF_2				X			n.d.
II	X	X	X	X		X	
$KAlF_4$–ZrF_4(2)				X	X	X	
$KAlF_4$–ZrF_4(3)*				X	X	X	

[a] I, undoped intermediate precipitate; II, ZrF_4-doped intermediate precipitate; *, melted under HF; n.d., not detected.

TABLE II

Material	Preparation ambient	A	A′	B	B′	C
		H_2O (cm^{-1})		OH_F^x (cm^{-1})		(cm^{-1})
I	H_2O/air	3450, 3220[a]	1690			740
$KAlF_4$	air			3480	1670	750
$KAlF_4$–ZrF_4(1)	air			3480		745
$KAlF_4$–BaF_2	air			3470		745
II	H_2O/air	3450	1690			740
$KAlF_4$–ZrF_4(2)	air			3480		745
$KAlF_4$–ZrF_4(3)	HF			3480	1670	742

[a] Shoulder.

fraction BaF_2. A comparison of the X-ray fluorescence analyses of the standard mixtures and of a sample of $KAlF_4$–ZrF_4 (1) revealed 0.095 mole fraction of ZrF_4. The same amount of ZrF_4 has been used to dope the intermediate precipitate II (Table I). However, in materials (2) and (3) ZrF_4 is present as a separate phase.

B. Electrical Conductivity

In Fig. 3, the Arrhenius plots of $\log(\sigma T)$ versus $10^5/T$ at 1 kHz are presented for single crystals of undoped $KAlF_4$, both perpendicular and along the AlF_4^- layers, and for an undoped pellet of $KAlF_4$. Specific conductivity values of pressed pellets were not corrected for the deviations from the theoretical density (density values are included in the figure captions). At this frequency, the conductivities were independent of the a-c amplitude over the range employed. Results for pellets of undoped $KAlF_4$, $KA1F_4$–BaF_2, and $KaAF_4$–ZrF_4 (1) are presented in Fig. 4. Figure 5 presents the temperature dependence of $KAlF_4$ doped with ZrF_4 prepared in air from the doped intermediate precipitate II ($KAlF_4$–ZrF_4 (2)), and prepared in an atmosphere of HF ($KAlF_4$–ZrF_4 (3)). Values for the activation enthalpies as calculated from the experimental results are gathered in Table III.

The experimental results indicate that the electrical conductivity of $KAlF_4$ is increased at lower temperatures upon doping with either ZrF_4 or the BaF_2–AlF_3 mixture. In comparison with the results for the BaF_2-doped samples, the increase of the conductivity for the ZrF_4-doped samples is less than expected from the amount of dopant material present.

The temperature dependence of the conductivity at lower temperatures of samples $KAlF_4$–ZrF_4 (2) and (3) was appreciably different from that of the undoped material. In order to get additional information on the

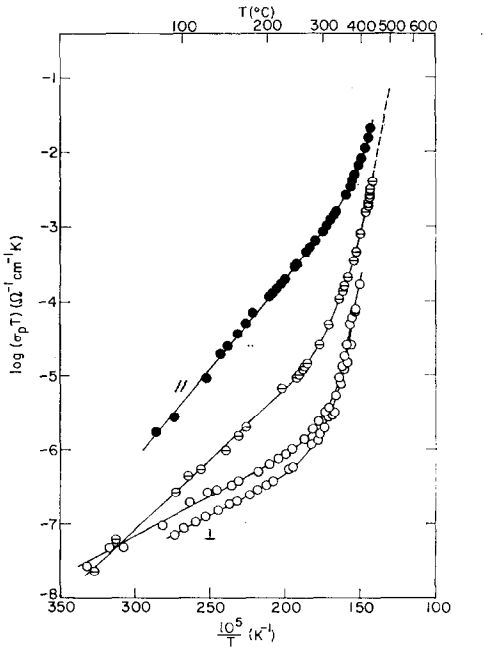

FIG. 3. Electrical conductivity of undoped $KAlF_4$ at 1 kHz, plotted as $\log(\sigma_p T)$ versus $10^5/T$. ○○, $KA1F_4$ ⊥ layers (∥ c-axis), 2 different crystals; ●●, $KAlF_4$ ∥ layers (⊥ c-axis); ⊖⊖, $KAlF_4$ pellet (79%).

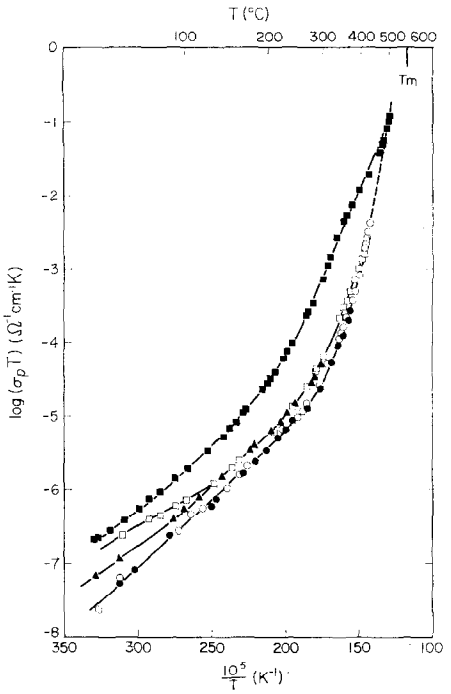

FIG. 4. Electrical conductivity of undoped and doped $KAlF_4$ pellets at 1 kHz. ○,●, undoped $KAlF_4$ (79%, 79%); △, □, $KAlF_4$–ZrF_4 (1) (82, 79%). ■, $KAlF_4$–BaF_2 (76%).

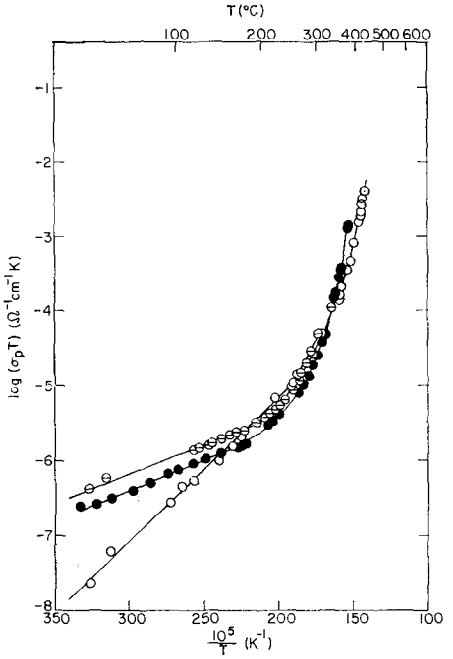

FIG. 5. Electrical conductivity of undoped and ZrF_4-doped $KAlF_4$ at 1 kHz. ○, undoped $KAlF_4$ (79%); ●, $KAlF_4$–ZrF_4 (2) (air) (72%); ⊖, $KAlF_4$–ZrF_4 (3) (HF) (68%).

mobile species in these ZrF_4-doped samples, transference number measurements were performed on pellets of $KAlF_4$–ZrF_4 (2). The high resistance of these samples made practical use of the cell arrangement as given in Fig. 2 possible only at temperatures above about 300°C. All pellets were preheated at 450°C for 20 hr in a dry oxygen-free argon atmosphere before the transference number measurements. At 314 and 322°C, 300 mV was applied for about 15 hr. The weights of pellets 2, 4, and 8 remained unchanged (weight loss <0.2 mg). Unfortunately, good separation between the pellets required q values not larger than 1C, leading to considerable uncertainties in the transference numbers. At the experimental temperatures we obtained the value 0.17 ± 0.06 for t_F^- by direct measurement. However, one can also infer values of the transference number from the results presented in Fig. 5 by extrapolating the low temperature extrinsic conductivity, which we assume is due to F^- transport, and comparing it with the measured total conductivity. By doing so, we obtain values of 0.11 at 314°C and 0.08 at 322°C.

TABLE III

CONDUCTIVITY ACTIVATION ENTHALPIES FOR UNDOPED $KAlF_4$ AT 1 kHz

Sample	ΔH_1 (eV)	ΔH_2 (eV)
$KAlF_4$ (∥)[a]	0.49	1.5
$KAlF_4$ (⊥)[a]	0.22	2.3
$KAlF_4$ (pellet)	0.38	2.1

[a] ∥ and ⊥ to the layer.

For further evaluation of the transport phenomena in this system the frequency dependence of the a-c electrical response of these materials was investigated. All samples investigated in the temperature region 300–450°C showed a frequency-independent conductivity over the range 0.8–20 kHz, whereas

for a BaF_2-doped sample the lower temperature limit was about 200°C.

At temperatures lower than 300°C the conductivity is frequency dependent, in that G_p increases with increasing frequency, whereas C_p decreases upon increasing the frequency. Figure 6 presents an example of the frequency dependence of G_p and C_p. A display of a typical result upon the complex admittance plane is presented in Fig. 7.

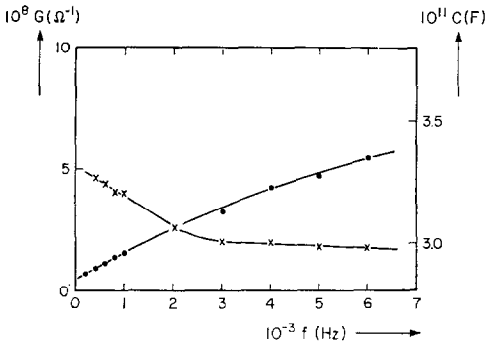

FIG. 6. Frequency dependence of apparent parallel conductance (G_p, circles) and capacitance (C_p, crosses) of $KAlF_4$–ZrF_4 (2) at $T = 167$°C.

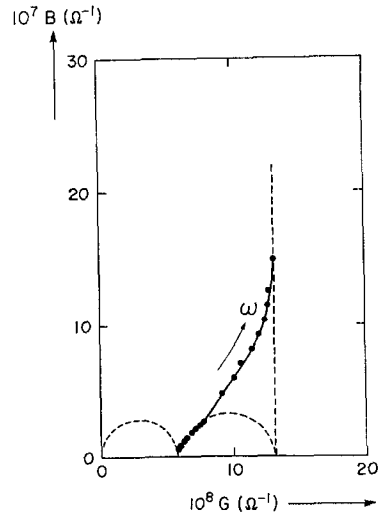

FIG. 7. Complex plane admittance plot of undoped $KAlF_4$ at 269°C. Frequency range, 0.20–13 kHz.

The observation of frequency-independent conductivities means that in the high temperature regime the sample–electrode system can be represented by a simple equivalent circuit, with the bulk resistance and interfacial capacitance in parallel with the geometric, or high-frequency, capacitance. From the data, the geometric capacitance was found to be 14.8–16.7 pF for both undoped and doped specimens, independent of temperature.

This simple equivalent circuit predicts that upon applying step voltage d-c currents at $t = 0$ sec, would give conductivity values equal to those obtained with high frequency a-c measurements, since the sudden imposition of a potential step is equivalent to the use of a very high frequency. On applying 120 mV across the BaF_2-doped sample, placed between blocking electrodes, polarization currents decayed to zero current within a few minutes at $T = 292$°C, indicating negligible electronic conduction. Polarization times increased at decreasing temperatures. The conductivities calculated from $i(t = 0)$ values are presented in Fig. 8. These results support this simple series–parallel equivalent circuit at high temperatures.

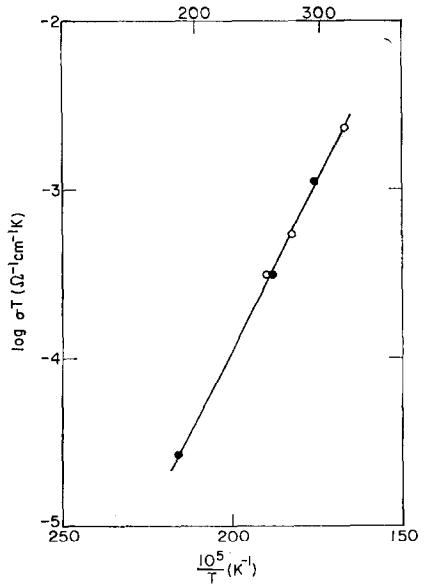

FIG. 8. Specific conductivities of $KAlF_4$–BaF_2 (75%) at 1 kHz (○) and as calculated from $i(t = 0)$ (●).

4. Discussion

A. Compositional Considerations

Upon heating, the intermediate precipitates I and II, $K_2AlF_5 \cdot H_2O$ will dehydrate and KHF_2 will decompose. Before the melting temperature of the intermediate precipitate, which in fact is a mixture, is reached, solid state reaction between KF and $KAlF_4$ is possible (*8*) leading to K_3AlF_6 contamination.

If stoichiometric proportions of KF and AlF_3 are used in the preparation of $KAlF_4$ then the solidified melt should consist of

$$(1 - \tfrac{3}{2}\delta)KAlF_4 + \tfrac{1}{2}\delta K_3AlF_6 + \delta AlF_3. \quad (5)$$

One may expect that an excess of AlF_3 is more soluble in $KAlF_4$ than is an excess of KF, since in the former case a set of vacancies is formed, whereas an excess of KF leads to a set of interstitial defects. In fact, the X-ray diffraction results of the compounds $KAlF_4$–ZrF_4 (2) and (3) (Table I) support this assumption, since AlF_3 was not detected while K_3AlF_6 was. This then should lead to a host lattice with the composition

$$KAlF_4 + \delta AlF_3 = (K_K^x)\,(V_K')_\delta\,(Al_{Al}^x)_{1+\delta} \times (F_F^x)_{4+3\delta}\,(V_F^\cdot)_\delta \quad (6)$$

with the electroneutrality condition

$$[V_F^\cdot] = [V_K']. \quad (7)$$

The compositions of the materials $KAlF_4$–ZrF_4 (2) and (3) may then be represented by

$$KAlF_4(\delta AlF_3) + \gamma ZrF_4 = (K_K^x)\,(V_K')_{\delta+\gamma}\,(Al_{Al}^x)_{1+\delta}\,(Zr_{Al}^\cdot)_\gamma \times (F_F^x)_{4(1+\gamma)+3\delta}\,(V_F^\cdot)_\delta \quad (8)$$

with the electroneutrality condition

$$[Zr_{Al}^\cdot] + [V_F^\cdot] = [V_K']. \quad (9)$$

Since both K_3AlF_6 and ZrF_4 were present as a separate phase it seems that in these materials $\gamma < \delta$, which means that the concentration of fluoride ion vacancies cannot be neglected in these materials.

In view of previously reported (*2*) doping experiments on Na_3AlF_6, BaF_2 should be more soluble in $KAlF_4$ in the presence of a proper amount of AlF_3. In additon to γ BaF_2 an amount of 2γ AlF_3 was added during the preparation. This should yield a material of composition

$$KAlF_4 + \gamma BaF_2 + 2\gamma AlF_3 = (K_K^x)\,(Ba_K^\cdot)_\gamma (V_K')_\gamma\,(Al_{Al}^x)_{1+2\gamma}\,(F_F^x)_{4(1+2\gamma)} \quad (10)$$

with the electroneutrality condition

$$[Ba_K^\cdot] = [V_K']. \quad (11)$$

The composition of $KAlF_4$–ZrF_4 (1) can be represented by composition (8) with $\delta = 0$, and with the electroneutrality condition

$$[Zr_{Al}^\cdot] = [V_K']. \quad (12)$$

A slight excess of AlF_3, and thus the presence of K_3AlF_6, would yield for BaF_2 doped $KAlF_4$ the composition

$$(K_K^x)\,(Ba_K^\cdot)_\gamma\,(V_K')_{\gamma+\delta}\,(Al_{Al}^x)_{1+2\gamma+\delta} \times (F_F^x)_{4(1+2\gamma)+3\delta}\,(V_F^\cdot)_\delta. \quad (13)$$

From the results in Table I one may conclude that for the materials $KAlF_4$–BaF_2 and $KAlF_4$–ZrF_4 (1) $\gamma > \delta$ holds.

Use of Brosset's method to prepare $KAlF_4$ invariably leads to contamination due to hydrolysis at higher temperatures. Even our hydrofluorinated samples showed the presence of OH^- ions. The formation of oxide impurities at higher temperatures and during the melting procedure seems likely, and leads to fluoride ion vacancies through

$$F_F^x + OH_F^x \rightarrow O_F' + V_F^\cdot + HF. \quad (14)$$

Therefore, the general total electroneutrality condition is

$$[Zr_{Al}^\cdot] + [Ba_K^\cdot] + [V_F^\cdot] = [V_K'] + [O_F']. \quad (15)$$

B. Ionic Conductivity

The electrical conductivity of $KAlF_4$ is highly anisotropic. The conductivity in the layers normal to the *c*-axis is larger than the conductivity in the *c*-axis direction. The ionic conductivity of the materials $KAlF_4$–BaF_2 and $KAlF_4$–ZrF_4 (1), which is larger than the conductivity of undoped $KAlF_4$ over an appreciable temperature region corresponds

with (10), while (8) with $\delta = 0$ seems inadequate to explain the low conductivity of the ZrF_4-doped sample. If not δ AlF_3 but δ KF is present in a small excess as a separate phase, we may assume incorporation of δ $KZrF_5$ and (γ-δ) ZrF_4, where γ denotes the total amount of added ZrF_4. The electroneutrality condition then reads $[V_K'] + [F_i'] = [Zr_{Al}]$. Differentiation between composition (8) with $\delta = 0$ and a composition containing an excess δ of KF cannot be made on the basis of X-ray diffraction data.

In the high-temperature region, the conductivity of the samples reflects intrinsic behavior. The low-temperature conductivity of the materials $KAlF_4$–ZrF_4 (2) and (3) is governed by fluoride ion motion, while in the high-temperature region potassium ion conduction predominates, in line with composition (8).

From the conductivity results, we may conclude that intrinsic defects in $KAlF_4$ are generated according to

$$K_K^x + V_i^x \rightleftarrows K_i^{\cdot} + V_K', \quad \text{with } K = [K_i^{\cdot}]\,[V_K']. \qquad (16)$$

The low conductivity activation enthalpy ΔH_1 for $KAlF_4$ ($\perp$) (Table III) is comparable to the value obtained for materials $KAlF_4$–ZrF_4 (2) and (3), and therefore suggests fluoride conduction via fluoride ion vacancies, either present due to O_F' or a deviation from stoichiometry. The value for ΔH_1 for $KAlF_4$ ($\parallel$), being larger than the value for ΔH_1 for $KAlF_4$ ($\perp$) indicates potassium conduction. From ΔH_2 ($\parallel$), we obtain a value of 2.0 eV for the formation enthalpy of the intrinsic defect pair V_K', $K_i^{\cdot}$. Since a formation enthalpy is an intrinsic property of a compound, its value is assumed to be independent of crystallographic anisotropies. ΔH_2 for $KAlF_4$ ($\perp$) then leads to a migration enthalpy for potassium ion vacancies perpendicular to the layers of about 1.3 eV.

Maycock and Pai Verneker (*9*) found a linear relationship between formation enthalpies and melting temperatures for a series of binary as well as ternary potassium, lithium and silver salts, exhibiting Schottky or Frenkel disorder. Their empirical relation predicts for the formation enthalpy for intrinsic defects in $KAlF_4$ the value 1.86 eV, which is in reasonable agreement with the value of 2.0 eV estimated from the data.

From the crystal structure of $KAlF_4$ (Fig. 1) and the ionic radii of F^- (1.33 Å) and K^+ (1.51 Å), we can calculate the sizes of the apertures through which the two types of ions must pass in order for motion to occur in the *c* direction. The aperture for F^- ions is at ($\frac{1}{2}$ $\frac{1}{2}$ 0), and has a radius of 1.0 Å. The K^+ ion aperture is at (0 0 $\frac{1}{2}$), and has a radius of 0.45 Å.

Likewise, in the direction normal to the *c*-axis, and parallel to the layers, the K^+ ions may move through an aperture at ($\frac{1}{2}$ 0 0), which has a radius of 0.87 Å.

From these considerations and the ionic conductivity results, we arrive at the conclusion that the anisotropy in fluoride ion motion is less than is the case for potassium ion motion, and that the mobility of $V_F^{\cdot}$ is greater than that of V_K' normal to the layers. The results on the single crystals then suggest that parallel to the layers (normal to the *c*-axis), V_K' has a greater mobility than $V_F^{\cdot}$.

C. Frequency Dependence of the Conductivity

The admittances of the nominally pure and doped samples showed a frequency dispersion in the low-temperature region, as presented in Fig. 7. The increase in *G* over the frequency range employed differed at constant temperature from sample to sample. At lower temperatures the frequency dependence of *G* became more pronounced.

Although surface roughness at the electrodes might be of influence (10), we are inclined to believe that an interparticle resistance larger than the resistance of the crystallites is responsible for the observed frequency dispersion of the samples. This leads to an additional grain boundary resistance in series with the ionic resistance of the bulk electrolyte. Since the average interionic distance within the grain boundary region is greater than in the crystal, we can model the grain boundary as a thin air-gap capacitor in series with the bulk of the electrolyte and shunted by the grain boundary resistance. We then obtain the equivalent circuit given in Fig. 9. To interpret the a-c

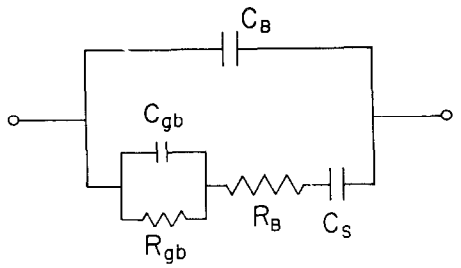

FIG. 9. Equivalent circuit for a pressed pellet with interparticle resistance. R_B and C_B represent the bulk resistance and capacitance. R_{gb} and C_{gb} represent the grain boundary resistance and capacitance. C_S is the double-layer capacitance.

experiments in terms of this equivalent circuit is is desirable to express the results in terms of the real and imaginary parts of the complex admittance

$$Y = G + jB. \tag{17}$$

For this case, G, the apparent parallel conductance, can be expressed by

$$G = \frac{\omega^4 C_{gb}^2 C_S^2 G_B + \omega^2 C_S^2 G_{gb} G_B^2 + \omega^2 G_{gb}^2 G_B C_S^2}{(G_{gb} G_B - \omega^2 C_{gb} C_S)^2 + \omega^2 (C_S G_B + C_S G_{gb} + C_{gb} G_B)^2} \tag{18}$$

and the apparent parallel capacitance is given by

$$C = B/\omega = \frac{\omega^2 C_{gb} C_S^2 G_B^2 + \omega^2 C_{gb}^2 C_S G_B^2 + G_{gb}^2 G_B^2 C_S}{(G_{gb} G_B - \omega^2 C_{gb} C_S)^2 + \omega^2 (C_S G_B + C_S G_{gb} + C_{gb} G_B)^2} + C_B. \tag{19}$$

With $C_S \gg C_{gb} \gg C_B$, and G_B and G_{gb} of the same order of magnitude, one obtains data in the complex plane as indicated by the dashed curve in Fig. 7.

With the assumptions $R_{gb} \sim 10\ R_B$ (R_B value at the highest frequency used), $C_{gb} \sim 1.7\ C_B = 10^{-11}$ F, and $C_S = 10^{-6}$ F, then curves such as those given in Fig. 6 and 7 can be generated in the frequency range 0.2–20 kHz. The equivalent circuit given in Fig. 9 means that conductivity measurements at 1 kHz should yield lower apparent conductivities (at least in parts of the extrinsic conductivity region) than expected for true bulk properties. Such behavior is indicated by the transference numbers for fluoride ions in material $KAlF_4$–ZrF_4 (2), since t-values obtained from the extrapolated extrinsic conductivity measured at 1 kHz and the total conductivity are smaller than the experimental t_F- values.

Since no systematic study was made of each material over an appreciable temperature region, the temperature dependence of R_B and R_{gb} could not be extracted separately from the data.

One of the implications is that an interpretation of the conductivity of $KAlF_4$–BaF_2 and $KAlF_4$–ZrF_4 (1) in the region RT – 150°C in terms of the contribution due to fluoride ion vacancies based on composition (13) or composition (8) with $\delta \neq 0$, should await a detailed study into R_{gb}.

5. Conclusions

Studies of the chemical and physical properties of $KAlF_4$ have often used Brosset's method to prepare the material. The present study reveals that this preparation method may lead to uncontrolled deviations from stoichiometry.

Although the conductivity results indicate intrinsic Frenkel defect formation in the potassium ion sublattice and potassium conduction via potassium ion vacancies at higher temperatures, fluoride ion conduction via vacancies seems to govern the charge transport process at lower temperatures. This behavior originates from the deviations from the stoichiometric composition and is directly related to the lamellar crystal structure of $KAlF_4$. In this lower temperature region, grain boundary effects begin to appear and interfere with the determination of the transport parameters within the crystal lattice. To determine accurately the conduction by fluoride ion vacancies and the relation between composition and conductivity at low temperatures, the use of single crystals is necessary.

Acknowledgments

The authors are grateful to Dr. L. E. Nagel for computer simulations of the behavior of equivalent

circuits in the complex plane. This work was supported by the Office of Naval Research and the Advanced Research Project Agency.

References

1. G. J. LANDON AND A. R. UBBELOHDE, *Proc. Roy. Soc. (London)* **240**, 160 (1957).
2. E. W. DEWING, *Trans. Met. Soc. AIME* **245**, 1829 (1969).
3. J. SCHOONMAN AND R. A. HUGGINS, to appear.
4. C. BROSSET, *Z. Anorg. Allg. Chem.* **239**, 301 (1938).
5. C. BROSSET, Ph.D. Thesis, Stockholm (1942).
6. J. LECOMPTE, C. DUVAL, AND C. WADIER, *Comp. Rend.* **249**, 1991 (1959).
7. S. D. Ross, "Inorganic Infrared and Raman Spectra", p. 198, McGraw-Hill, New York (1972).
8. B. PHILLIPS, C. M. WARSHAW, AND I. MOCKRIN, *J. Amer. Ceram. Soc.* **49**, 631 (1966).
9. J. N. MAYCOCK AND V. R. PAI VERNEKER, *Phys. Status Solidi (B)* **44**, 97 (1971).
10. R. D. ARMSTRONG, T. DICKINSON, AND P. M. WILLIS, *J. Electroanal. Chem.* **53**, 389 (1974).